Massive Multi-Mission Statistical Study and Analytical Modeling of the Earth's Magnetopause: 4. On the Near-Cusp Magnetopause Indentation

G. Nguyen, N. Aunai, Bayane Michotte de Welle, A. Jeandet, B. Lavraud, D. Fontaine

JGR Space Physics

RESEARCH ARTICLE
10.1029/2021JA029776

Massive Multi-Mission Statistical Study and Analytical Modeling of the Earth's Magnetopause: 4. On the Near-Cusp Magnetopause Indentation

G. Nguyen[1,2], N. Aunai[1], B. Michotte de Welle[1], A. Jeandet[1], B. Lavraud[3,4], and D. Fontaine[1]

[1]CNRS, Ecole Polytechnique, Sorbonne Université, University Paris Sud, Observatoire de Paris, Institut Polytechnique de Paris, Université Paris-Saclay, PSL Research Univsersity, Laboratoire de Physique des Plasmas, Palaiseau, France, [2]Direction Generale de L'Armement, Paris, France, [3]Institut de Recherche en Astrophysique et Planétologie, Université de Toulouse, CNRS, CNES, Toulouse, France, [4]Laboratoire D'astrophysique de Bordeaux, University Bordeaux, CNRS, Toulouse, France

Abstract The shape and location of the magnetopause current sheet in the near-cusp region is still a debated question. Over time, several observations led to contradictory conclusions regarding the presence of an indentation of the magnetopause in that region. As a result several empirical models consider the surface is indented in that region, while some others do not. To tackle this issue, we fit a total of 17,230 magnetopause crossings to various indented and non-indented analytical models. The results show that while all models describe the magnetopause position and shape equivalently far from the cusp region, the non-indented version over-estimate the radial position of the near-cusp magnetopause. Among indented models, we show that the one designed from non-linearmagneto hydrodynamic simulations fits well the near-cusp magnetopause location, while the other underestimate its position probably because their design was possibly based on magnetopause crossing catalogs that contain cusp inner boundary crossings.

This article is a companion to Nguyen et al. (2022a), https://doi.org/10.1029/2021JA029773; Nguyen et al. (2022b), https://doi.org/10.1029/2021JA029774; and Nguyen et al. (2022c), https://doi.org/10.1029/2021JA030112.

Key Points:

- We compare the performances of several magnetopause models to investigate the near-cusp magnetopause shape
- Previous models of the near-cusp magnetopause indentation actually depicts the position of the cusp inner boundary
- We show that the actual magnetopause is indented and that the indentation is consistent with the one observed in non-linearmagneto hydrodynamic simulations

Correspondence to:

G. Nguyen,
gautier-mahe.nguyen@intradef.gouv.fr

Citation:

Nguyen, G., Aunai, N., Michotte de Welle, B., Jeandet, A., Lavraud, B., & Fontaine, D. (2022). Massive multi-mission statistical study and analytical modeling of the Earth's magnetopause: 4. On the near-cusp magnetopause indentation. *Journal of Geophysical Research: Space Physics*, *127*, e2021JA029776. https://doi.org/10.1029/2021JA029776

Received 9 JUL 2021
Accepted 8 DEC 2021

1. Introduction

The polar cusps are defined in the two terrestrial hemispheres as the two funnel-like regions near the poles of Earth's magnetic field. These regions, located at an average latitude of 75°, are the privileged entry place of solar particles in the magnetosphere as this was confirmed by the low-latitude IMP5 data observations of Frank (1971) and ISIS data observations of Heikkila and Winningham (1971).

Just like the different regions and boundaries of the near-Earth environment, the physical and geometrical properties of the cusps are strongly affected by the solar wind conditions and in particular by changing Interplanetary Magnetic Field (IMF) orientations.

When the IMF is northward (right panel of Figure 1), the cusp is shifted poleward (as suggested by the observational investigations of Nguyen et al. (2022d) and references therein). Magnetic reconnection occurs in the magnetosphere lobes and magnetic flux is convected sunward as shown with the green line of Figure 1 right panel. This convection, opposed to the tailward magnetosheath flow, generates a region of dense, overall stagnant plasma, hotter than the shocked solar wind and characterized by a low magnetic field amplitude. This region has been defined as the *exterior cusp* in Lavraud et al. (2002). A crossing of this region during northward IMF by the Cluster one spacecraft is shown between the two black lines in Figure 2.

When the IMF is southward (left panel of Figure 1), the cusp is shifted equatorward (as suggested by the observational investigations of Nguyen et al. (2022d) and references therein). Reconnection occurs on the dayside low latitude magnetopause. The merged field lines are convected tailward (green line). In this case, the direction of both the magnetoseath and reconnection flows are similar and the associated exterior cusp, still dense, hot and with a low magnetic field amplitude, becomes a region of overall tailward convection (Lavraud, Fedorov, et al., 2004; Lavraud, Phan, et al., 2004). A crossing of this region by the Cluster 1 spacecraft during southward IMF is shown between the two black lines in Figure 3.

In both cases this exterior cusp region causally results from the opening of the low-latitude or lobe reconnection outflow within which lies the main magnetopause current sheet associated to the kinked field lines convected tailward or sunward, respectively. In the exterior cusp, as the kink gradually diminishes, the magnetopause current sheet becomes less obvious to observe. Nevertheless, spacecraft data reveals a so-called *external boundary*

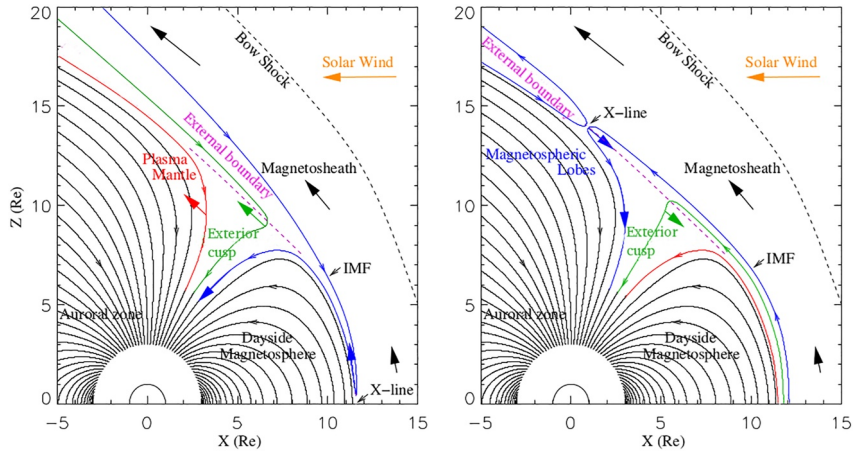

Figure 1. Schematic representation of the magnetic field topology and plasma flow in the near-cusp region for southward (left) and northward (right) Interplanetary Magnetic Field. The blue green lines show the time evolution of the reconnected field lines (see text). The red-line is the first non-convected field line and the dashed purple line represents the assumed location of the cusp external boundary (adapted from Lavraud and Cargill (2005)).

to the cusp, marking the transition between the exterior cusp and the magnetosheath proper. Outbound crossings (Lavraud, Phan, et al., 2004) are characterized by a rotational-like variation of the magnetic field orientation, an increased magnetic field and flow amplitudes, increased density along with a temperature decrease, as depicted as dotted lines in Figures 2 and 3.

The exterior cusp region is also bounded by two inner boundaries, which are not the continuation of the low-latitude or lobe magnetopause current sheet. These inner boundaries rather mark the transition with the nightside lobe and the dayside magnetosphere. Under southward IMF conditions, the transition from the exterior cusp with the dayside magnetosphere delimits the open-close field line separatrix, whereas the exterior cusp/lobe boundary is a more diffuse transition towards the lobe, as the flux tubes get emptied of reconnected plasma. Under northward IMF, the transition with the lobe is the magnetic reconnection separatrix while the dayside inner boundary is the location where the sunward convected plasma hits the strong dayside dipole field. The crossing of one of these inner boundaries is shown by the black dashed lines in the 2 and 3. Detailed analysis of these boundaries can be found in Lavraud et al. (2005); Lavraud and Cargill (2005).

The way to model the location and shape of the magnetopause in this region, ensuring the continuity between the day and night sides of the magnetosphere, has not yet reached a consensus.

The theoretical work of Spreiter and Briggs (1962) predicts a magnetopause indented earthward in this region as a result of pressure balance. However the model does not factor in reconnection, which is always occurring one way or another at the magnetopause and which is central to the formation of the boundaries as described above.

An indentation of the magnetopause was observationally suggested by Haerendel et al. (1978) with HEOS data. From then on, an apparent near-cusp indentation was also inferred in a multitude of studies based on data of various spacecraft (Boardsen et al. (2000); Šafránková et al. (2002) and references therein). Although somewhat a mainstream idea at this point, the existence of the indentation was once more questioned by the analysis of Hawkeye cusp data by Zhou and Russell (1997). The former suggesting its non-existence while the latter, although using the same observational data, suggesting the contrary. Using Cluster observations, Lavraud, Fedorov, et al. (2004) suggested that previous studies actually were inferring indentation from the crossings of the inner cusp boundaries, and that no statistical evidence of the external cusp boundary could be found.

Empirical analytical models fall into two categories and either do not present a magnetopause cusp indentation (Jelínek et al., 2012; Nguyen et al., 2022c; Shue et al., 1998) or do (Lin et al., 2010; Liu et al., 2015).

In this article, we revisit this long standing issue and question the indentation of the near cusp magnetopause current sheet as defined by the external cusp boundary, using the massive multi-mission magnetopause crossings

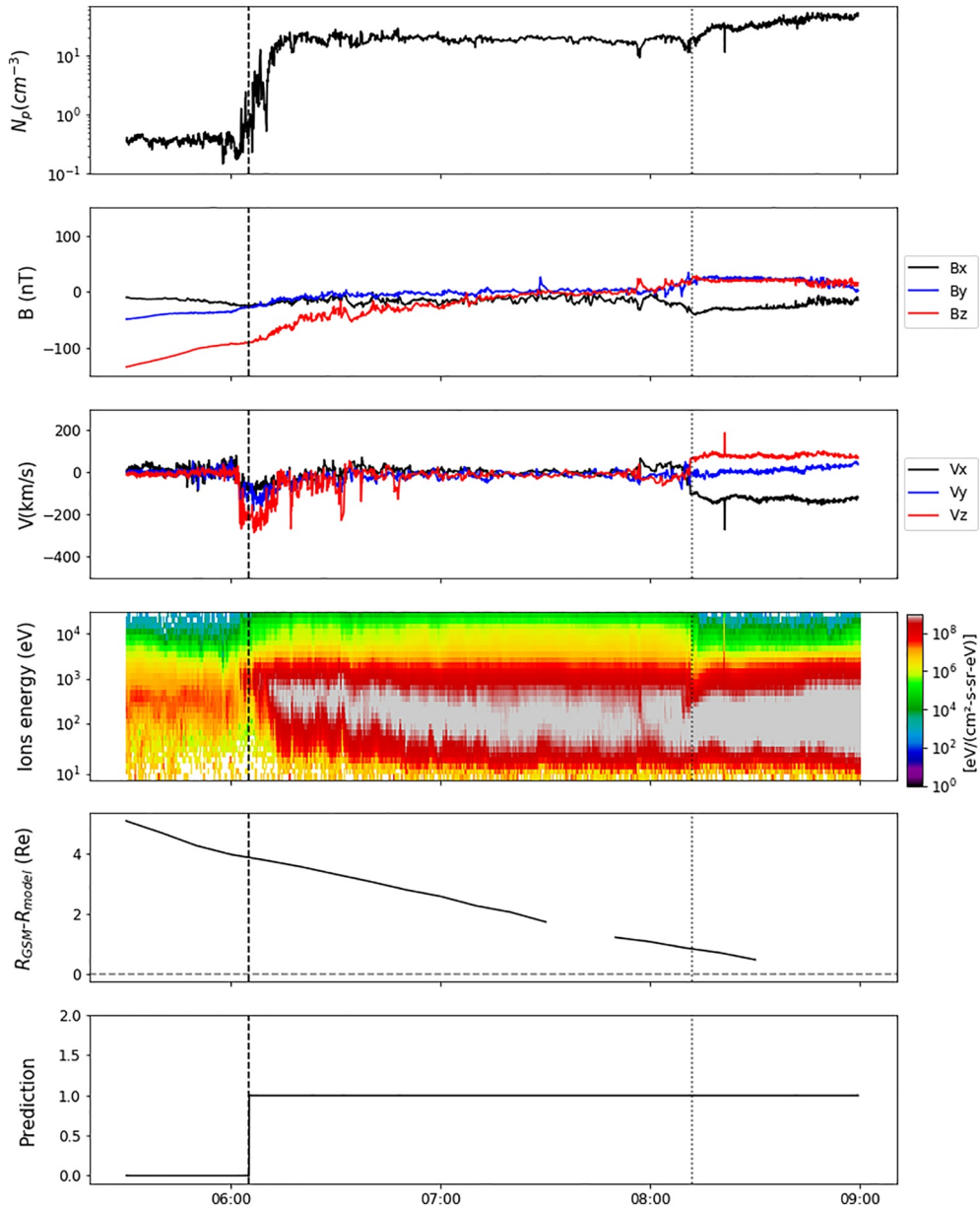

Figure 2. In-situ measurement provided by Cluster one spacecraft on the 16th of March 2002. From top to bottom are represented the ion density, the plasma magnetic field and velocity components, the omnidirectional energy fluxes of ions, The difference between the radial position of the spacecraft and the radial position predicted by the model of Nguyen et al. (2022c) and the prediction of the region classifier presented in Nguyen et al. (2022a). The black dashed line indicate the cusp inner boundary. The black dotted line indicate the cusp external boundary.

catalog presented in Nguyen et al. (2022a), one of the companion studies of this paper, along with an online accessible crossings database.

After a presentation of the crossings that we will be using, we will investigate the shape of the near-cusp magnetopause. We then adapt the non-indented magnetopause surface model developed in Nguyen et al. (2022c) to fit the indentation of the external boundary revealed by our statistical analysis.

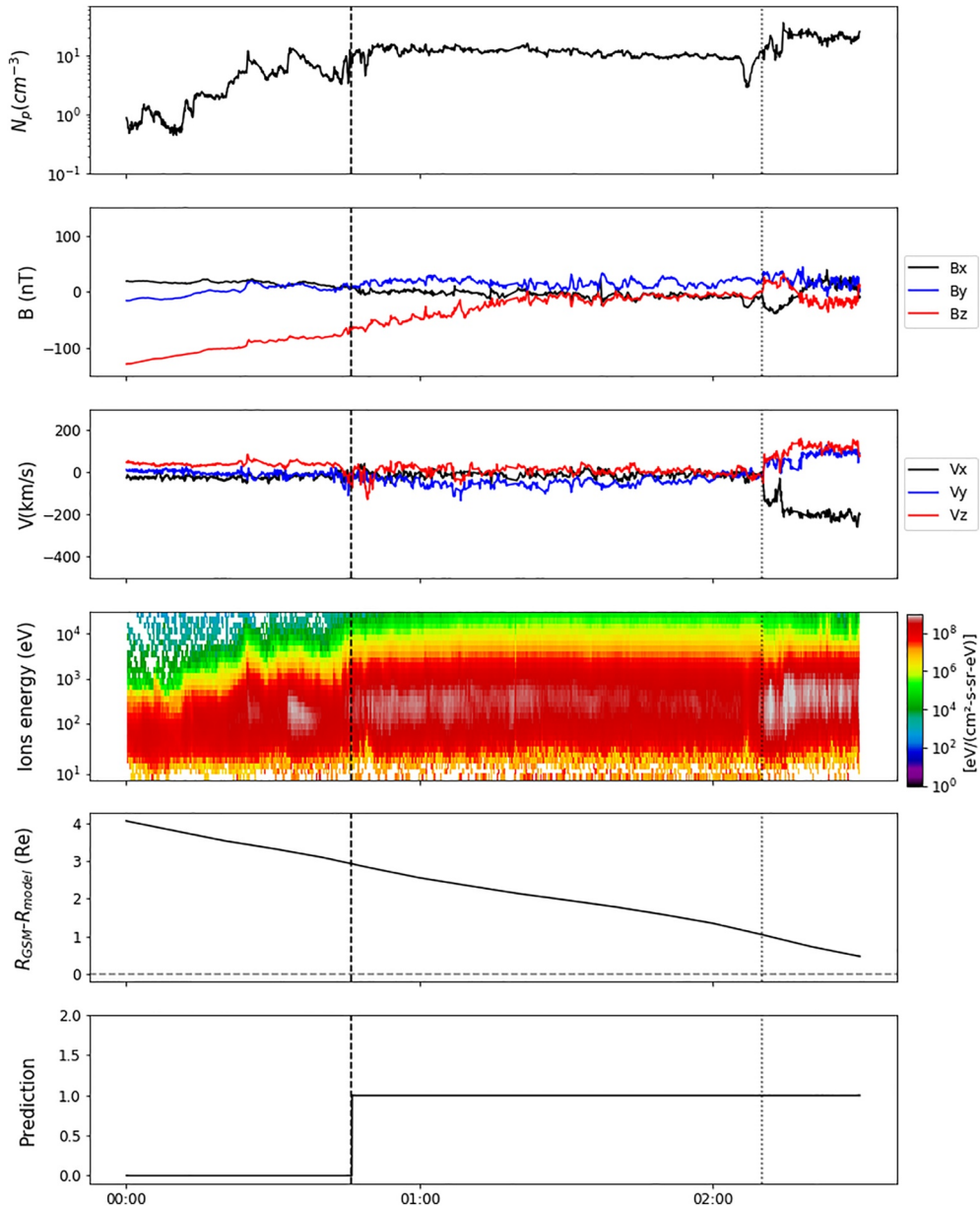

Figure 3. In-situ measurement provided by Cluster one spacecraft on the 21st of March 2002. The legend is the same than in Figure 2.

2. Data

2.1. Accessible Events Catalogs

We use the 15,062 magnetopause crossings automatically detected in Nguyen et al. (2022a) along with 2,168 online (ftp://nssdcftp.gsfc.nasa.gov/spacecraftdata/) crossings manually labeled. The former events correspond to magnetopause crossings detected in the in-situ data measurements of THEMIS, Cluster, Double Star, MMS and ARTEMIS with the help of a gradient boosting classifier. In the following, they will be designated as the *automatically detected crossings*. The latter events correspond to crossings of the missions IMP, ISEE, Geotail, Prognoz, Hawkeye, AMPTE, Explorer and OGO manually labeled by several observers. All of these crossings were used in the comparison of Liu et al. (2015)'s model to observational data and the Hawkeye crossings are the one used by Boardsen et al. (2000) and Lin et al. (2010) to study the shape of the near-cusp magnetopause. In the following, they will be designated as the *crossings from the NASA database*.

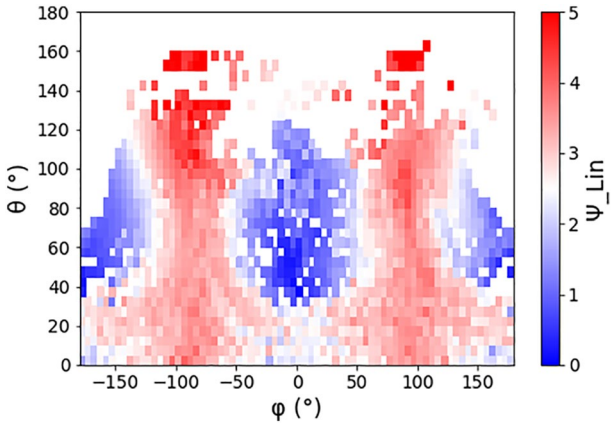

Figure 4. Binned average distribution of the Lin's distance Ψ_{Lin} of each crossing of our data set in the (ϕ, θ) plane.

Each crossing is then associated to a set of solar wind upstream conditions obtained with a temporal shift of OMNI data determined by applying the two-step propagation algorithm exposed in Šafránková et al. (2002). This determination of associated solar wind condition removed 1,394 automatically detected crossings for which no OMNI data was available.

We correct the GSM position of each of the obtained 15,836 magnetopause crossings by removing the aberration due to the Earth's revolution using a similar approach than what was done in Lin et al. (2010) and Boardsen et al. (2000) and assuming a revolution velocity of 30 km/s. In the following, the positions we consider will then be expressed in the so-called cGSM coordinate system.

2.2. Measuring the Distance to the Theoretical Expected Cusp Position

Following the description of the near-cusp region provided by Lin et al. (2010), we define the so-called *Lin's distance* Ψ_{Lin} of each crossing as:

$$\begin{cases} \Psi_{Lin} = \sqrt{\dfrac{(\theta-\theta_n)^2+\phi^2}{\left(\dfrac{-1}{d_n}\right)^{-2/a_{21}}}}, & \text{if } Z > 0 \\ \Psi_{Lin} = \sqrt{\dfrac{(\theta-\theta_s)^2+\phi^2}{\left(\dfrac{-1}{d_n}\right)^{-2/a_{21}}}}, & \text{if } Z \leq 0 \end{cases} \quad (1)$$

where θ and ϕ are the zenithal and the azimuthal position of a given event defined following the same convention as in Nguyen et al. (2022b), $d_{n,s} = a_{16} \pm a_{17}\gamma + a_{18}\gamma^2$, $\theta_{n,s} = a_{19} \pm a_{20}\gamma$, and a_{21} represent the scope, the zenithal position and the shape of the polar cusps, γ is the Earth dipole tilt angle and $a_{16} = 2.60$, $a_{17} = 0.832$, $a_{18} = -5.328$, $a_{19} = 1.103$, $a_{20} = -0.907$ and $a_{21} = 1.450$ are the corresponding coefficients fitted by Lin et al. (2010) are the corresponding coefficients fitted by Lin et al. (2010).

Figure 4 represents the binned average distribution of Ψ_{Lin} in the (ϕ, θ) plane for our data set. The zones where the near-cusp region is expected (e.g., $40° < \theta < 120°$ and $|\cos(\phi)| < \cos(\pi/4)$) are characterized by a low value of Ψ_{Lin}, typically below 2, that contrast the values typically observed in the equatorial plane ($|\phi| \sim 90°$) that are mostly above 3. Ψ_{Lin} then represents a distance in the angular ($\theta - \phi$) plane between a given crossing and the theoretical position of the northern or the southern polar cusps as defined by Lin et al. (2010). The crossings likely to be found in the near-cusp region are then expected to have a low Ψ_{Lin} while this distance is expected to be high for the events located in the equatorial plane, around the subsolar point or in the far nightside.

The automatically detected crossings were defined in Nguyen et al. (2022a) as 1 hr intervals that contained as many magnetosheath data points as magnetosphere data points. Nevertheless, the magnetosheath defined with the labeling method we presented there actually corresponds to the shocked solar wind . Consequently, the exterior cusp, generated by the convection of reconnected field lines, is also classified by the Gradient Boosting method as magnetosheath. An important part of automatically detected near-cusp magnetopause crossings are then very likely to be crossings of the cusp inner boundary. This is for instance the case for the two crossings presented in Figures 2 and 3 as shown with their last panel that represents the prediction of the region classifier. The actual magnetopause crossing in both cases is indeed the second vertical line, rather than the first one.

Naturally, this limits the exploitation of the automatically detected crossings in the frame of the study of the shape of the near-cusp magnetopause. To cope with it, we manually determine the position of the magnetopause current-sheet by visually inspecting the 1,112 Cluster crossings for which $\Psi_{Lin} < 2.5$. In the following, these crossings will be designated as the manually selected crossings while the events for which $\Psi_{Lin} \geq 2.5$ will still be called the out of the cusp automatically detected crossings.

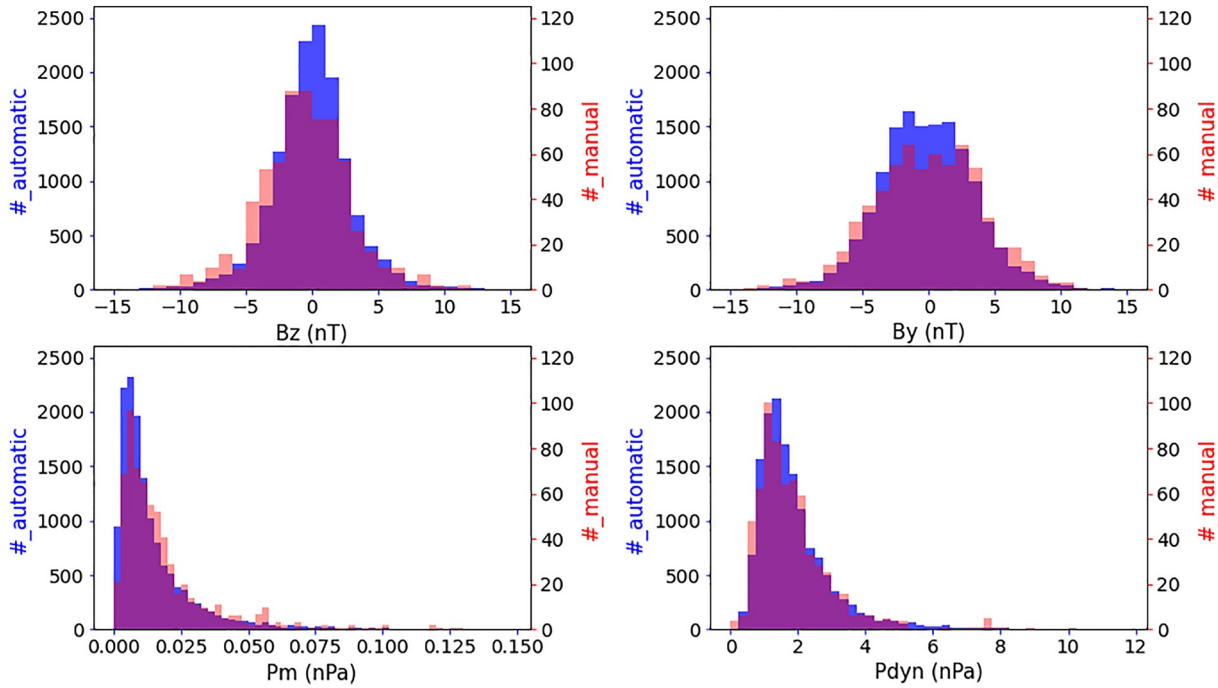

Figure 5. Histogram of the solar wind parameters of the automatically detected crossings (blue bins) and the manually selected crossings (red bins): the Interplanetary Magnetic Field B_y and B_z components (top row, right and left), the dynamic pressure P_{dyn} (bottom right), the magnetic pressure P_m (bottom, left).

2.3. Solar Wind Physical Parameters

The distributions of solar wind physical parameters associated to both the manually selected crossings and the automatically detected crossings are shown in the Figure 5. These distributions illustrate the conditions under which we expect the results of our study to be the most reliable. Although containing a significantly lower number of events, we notice similar distributions for both the automatically detected crossings (blue bins) and the manually selected events (red bins). Additionally, these histograms are similar to their OMNI counterpart. This shows that the greatest part of the two groups of crossings occurred under statistically regular solar wind conditions and that our manual selection of events is not biased by any of the considered solar wind physical parameter.

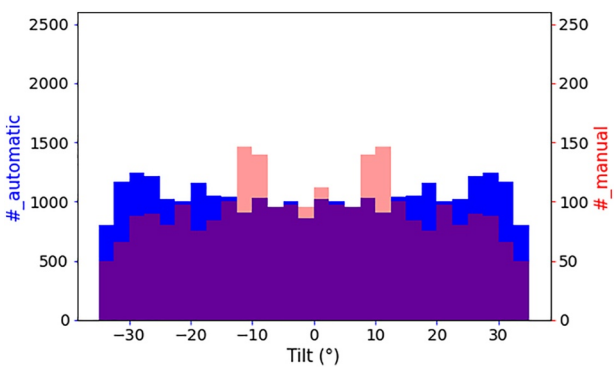

Figure 6. Histogram of the Earth dipole tilt angle associated to the symmetrized sets of the automatically detected crossings (blue bins) and the manually selected crossings (red bins).

2.4. Data Set Symmetrization

Following the symmetrization made in Nguyen et al. (2022b) and Nguyen et al. (2022c), we quadruple the size of the dataset by assuming first a similarity between the summer northern hemisphere and the winter southern hemisphere: $r\,(X, Y, Z, \gamma) = r\,(X, Y, -Z, -\gamma)$ and second a dawn-dusk symmetry of the magnetopause: $r\,(X, Y, Z) = r\,(X, -Y, Z)$.

The distribution of the Earth dipole tilt angle associated to the symmetrized sets of both the automatically detected crossings (blue bins) and the manually selected events (red bins) is shown in Figure 6. In the two cases, the symmetrization allows the data set to contain as many winter events as summer events and removes of a possible seasonal bias in the results of our study.

The final data set is then made of 54,672 automatically detected event, 4,448 manually selected crossings and 8,672 crossings from the NASA database.

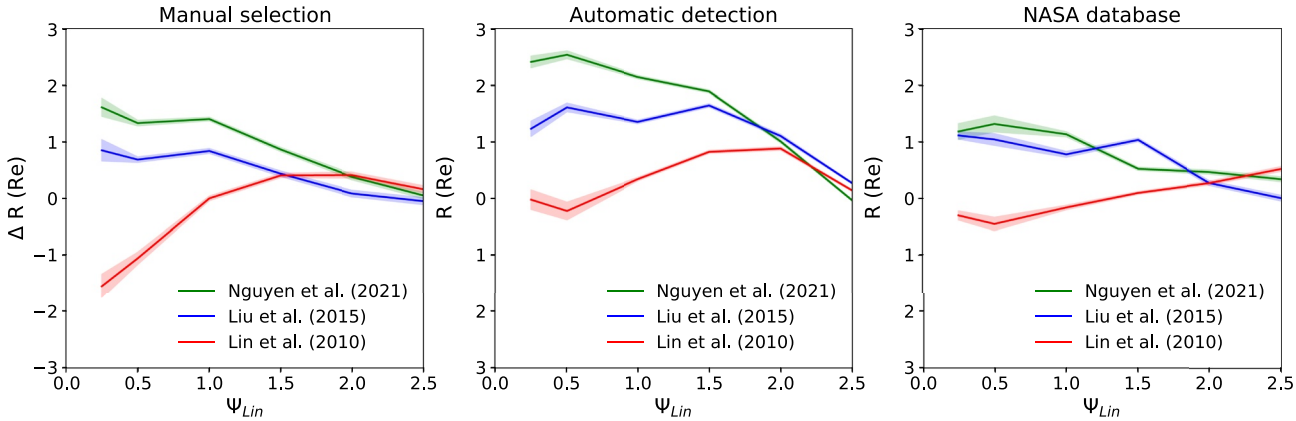

Figure 7. Evolution of the binned average error $\Delta R = R_{\text{model}} - R_{\text{observed}}$ of three models, Liu et al. (2015) *(blue)*, Lin et al. (2010) (*red*) and Nguyen et al. (2022b) (green) as a function of the Lin's distance Ψ_{Lin} on the manually selected crossings (left panel), the automatically detected crossings (*middle panel*) and the crossings from the NASA database (*right panel*). The colored shading represent the standard error of the mean associated to the local quadratic error of each model.

3. Shape of the Near-Cusp Magnetopause

Having made the distinction between the different families of events that constitute our data set, we can now focus on the position of the manually selected crossings in comparison to the position of the near-cusp crossings that originates from both the automatically detected events lists and the NASA database.

The left panel of Figure 7 represents the evolution of ΔR, the binned error between the model prediction R_{model} and the actual radial distance of a given crossing R_{observed}, as a function of Ψ_{Lin} on the manually selected crossings. The error of the non-indented model of Nguyen et al. (2022c) (green line) is positive and approaches to zero for the highest values Ψ_{Lin} that corresponds to the out of cusp crossings . This suggests their model overestimates the position of the magnetopause in the near-cusp region and is thus an argument in favor of indentation. Although also overestimating, the error of Liu et al. (2015)'s model is the lowest of the three models, which suggest this indentation could be appropriately described by the analytical expression they developed in their model. Nevertheless, these suggestions do not completely confirm the existence and the behavior of the indentation, this will be the objective of the next section.

It is also worth noting that the magnetopause model of Lin et al. (2010) seems to underestimate the position of the magnetopause for the lowest values of Ψ_{Lin}. This under-estimation could be explained by the fact they might have considered inner boundary crossings when fitting their model. The two other panels of Figure 7 represent the evolution of ΔR as a function of Ψ_{Lin} for the automatically detected events and the crossings from the NASA database respectively. For both panels, the models of Nguyen et al. (2022c) and Liu et al. (2015) overestimate the position of the two crossings population while Lin et al. (2010) tends towards negative errors within the cusp. In the case of the automatically detected crossings (*middle panel*), the error made by Nguyen et al. (2022c) and Liu et al. (2015) is higher than the one they made on the manually selected events. This indicates that the automatically detected crossings have, on average, a lower radial position than the manually selected ones. As detailed in the previous section, this radial difference can be explained by the fact that non negligible part of the automatically detected crossings might actually be inner boundary crossings. Since the error of the models on the crossings from the NASA database follows the same trend as the one of the automatically detected crossings, this suggests that the former event list also contains a significant part of inner boundary crossings, which may lead the fit of some analytical expression (Lin et al., 2010) to suggest an indentation of the magnetopause.

4. Fit of a New Indented Magnetopause Surface Model

The results shown in the previous section suggest a depletion of the near-cusp magnetopause that appears to be the most correctly described by the models obtained from the non-linear magnetohydrodynamic (MHD) simulations of Liu et al. (2015). We now go into more details to quantitatively assess the presence of a magnetopause indentation. Our methodology consists in finding the model that fits the best the crossing data set combining the manually selected cusp crossings and the automatically detected out of cusps ones.

A better fit of an indented model at every for every value of Ψ_{Lin} would then be a strong argument in favor of the actual existence of the near-cusp magnetopause indentation.

To do so, we fit three candidates models, described below, to the entire final data set made of the 54,672 out of cusp automatically detected event, the 8,672 out of cusp crossings from the NASA database and the 4,448 manually selected crossings and compare the fitting results of the three candidates. In the following We refer to this data set as the fitting data set.

4.1. Candidate Expressions

The three candidate models we will fit the data to actually correspond to adaptations of the non-indented expression of Nguyen et al. (2022c) to which is added an expression to take into account the description of a near-cusp indentation:

$$\begin{cases} r = r_0\left(\dfrac{2}{1+\cos(\theta)}\right)^{\xi} + Q \\ r_0 = a_0(P_{dyn}+P_m)^{a_1}(1+a_2\tanh(a_3 B_z)+a_4) \\ \xi = \xi_0 + \xi_1\cos(\phi) + \xi_2\cos(\phi)^2 + \xi_3\sin(\phi)^2 \\ \xi_0 = a_5 \\ \xi_1 = a_6\gamma \\ \xi_2 = a_7\cos(\Omega) \\ \xi_3 = a_8\cos(\Omega) \end{cases} \tag{2}$$

where r_0 describes the position of the magnetopause nose and Q the additive term that describes the indentation of the magnetopause. ξ_0 is the average level of flaring expected in the case of an axisymmetric magnetopause. ξ_1 describes the north-south asymmetry induced by seasonal variations through the variation of the dipole tilt angle γ . ξ_2 (resp. ξ_3) describes the variations of the magnetopause in the $(X-Z)$ (resp. $(X-Y)$) plane induced by the variations of the IMF cGSM B_z and B_y component through the variations of the IMF clock angle Ω. The coefficients a_i are the coefficients that will be determined by the fit to the fitting data set.

When $Q = 0$, the expression is exactly the one detailed in Nguyen et al. (2022c) and the model describes a non indented magnetopause surface. This is our first candidate model (named model 1).

The second candidate model (named model 2) expresses Q as the description of the near-cusp magnetopause provided by Lin et al. (2010):

$$\begin{cases} Q = C(\mathbf{e}^{d_n\psi_n^{a_{16}}} + \mathbf{e}^{d_s\psi_s^{a_{16}}}) \\ C = a_9(P_{dyn}+P_m)^{a_{10}} \\ d_{n,s} = a_{11} \pm a_{12}\gamma + a_{13}\gamma^2 \\ \psi_n = \arccos(\cos(\theta)\cos(\theta_n) + \sin(\theta)\sin(\theta_n)\cos(\phi)) \\ \psi_s = \arccos(\cos(\theta)\cos(\theta_s) + \sin(\theta)\sin(\theta_s)\cos(\phi-\pi)) \\ \theta_{n,s} = a_{14} \pm a_{15}\gamma \end{cases} \tag{3}$$

where C, d_n (d_s), a_{21} and θ_n (θ_s) control the depth, the scope, shape and location of the northern (southern cusp) indentation. Here, the near-cusp magnetopause is only parametrized by the dynamic and magnetic pressure, P_{dyn} and P_m along with the Earth dipole tilt angle γ. It is worth noting that this expression has the drawback of being

Table 1
Initial Values of the a_i Coefficients Used for the Fit of the Three Candidate Models Exposed in the Section 4.1

	Model 1	Model 2	Model 3
a_0	10.73	10.73	10.73
a_1	−0.150	−0.150	−0.150
a_2	0.0208	0.0208	0.0208
a_3	0.380	0.380	0.380
a_4	2.09	2.09	2.09
a_5	0.55	0.55	0.55
a_6	0.088	0.088	0.088
a_7	0.0150	0.0150	0.0150
a_8	−0.0870	−0.0870	−0.0870
a_9		−4.43	0.100
a_{10}		−0.636	0.822
a_{11}		−2.60	0.292
a_{12}		0.832	0.0879
a_{13}		−5.33	10.12
a_{14}		1.10	0.0128
a_{15}		−0.907	0.238
a_{16}		1.45	0.00581
a_{17}			0.00234

Table 2
Final Values of the a_i Coefficients of the Three Candidate Models After Performing a Fit to the Training Set

	Model 1	Model 2	Model 3
a_0	10.78	10.79	10.85
a_1	−0.150	−0.150	−0.150
a_2	0.0237	0.0357	0.0270
a_3	0.254	0.172	0.296
a_4	2.16	2.12	2.14
a_5	0.552	0.547	0.549
a_6	0.0671	0.0833	0.0745
a_7	0.0150	0.0150	0.0100
a_8	−0.168	−0.0704	−0.0713
a_9		−4.29	0.123
a_{10}		−0.403	0.877
a_{11}		−2.68	0.329
a_{12}		0.833	0.211
a_{13}		−5.33	10.13
a_{14}		1.19	0.464
a_{15}		−0.734	0.326
a_{16}		1.29	0.08355
a_{17}			0.00721

non-zero at the stand-off position of the magnetopause and in the nightside, biasing the interpretability we can have of r_0 that cannot anymore be considered as the representation of the stand-off position.

The third candidate model (named model 3) expresses Q as the description of the near-cusp magnetopause provided by Liu et al. (2015):

$$\begin{cases} Q = -a_9 C r_0 \left(\frac{2}{1+\cos(\theta)}\right)^{\xi} \cos(\phi)^2 \\ C = \mathbf{e}^{-\frac{|\theta - l_n|}{w}}(1+\text{sgn}(\cos(\phi))) + \mathbf{e}^{-\frac{|\theta - l_s|}{w}}(1+\text{sgn}(\cos(-\phi))) \\ l_{n,s} = (a_{10} + a_{11}\tanh[a_{12}(B_z + a_{13})])(1 \mp a_{14}\gamma) \\ w = (a_{15} + a_{16}\log(P_{dyn}))(1 + a_{17}\gamma^2) \end{cases} \quad (4)$$

where $l_{n,s}$ and w control the location and the angular width of the northern and southern cusps indentation respectively. In addition to the two pressures, the near-cusp magnetopause is parametrized by the IMF B_z component, which is consistent with an expected influence of a changing IMF orientation on the location of the polar cusps.

4.2. Fitting the Models

Following these descriptions, we fit the three candidate models to the final data set. To ensure the evaluation of the three fits measures the capacity each model has to generalize on unknown data, we randomly split the final data set into 45,195 *train set events* used to determine the values of the a_i coefficients in each model and 22,597 *test set events* actually used for their evaluation. The initial values of the different a_i coefficients are shown in the Table 1. These values are set equal to their numerical counterpart exposed in Lin et al. (2010); Liu et al. (2015) and Nguyen et al. (2022c) for the models 1, 2 and 3 respectively.

For each model, we then aply the Levenberg-Marquerdt fitting method (Newville et al., 2014) on the train set to determine the final values of the a_i coefficients shown in the Table 2. Although not shown, we performed the fits for several train-test splits but noticed very few variations of the value obtained for each coefficient a_i.

4.3. Evaluating the Models

Following the fitting phase, we evaluate the performance of the three obtained magnetopause surface models by measuring its Root Mean Square error (RMSE) on the 22,597 events of the test set. Although not shown, we performed the same evaluation for different training and test set and noticed no variations in our results. The evolution of the binned average RMSE of the three different models as a function of Ψ_{Lin} is shown in Figure 8.

First, it is worth noting that the global RMSE decreases with the introduction of an indentation term, the lowest RMSE being associated to model 3. This would have been a convincing argument in favor of a near-cusp indentation consistent with MHD simulations if the values of the global RMSEs were not so close.

The evolution of the local RMSE as a function of Ψ_{Lin} makes it actually clearer. Past the second dotted line, we notice similar values of the local RMSE of

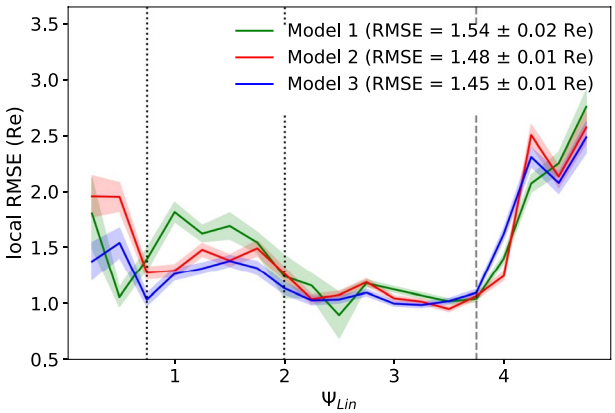

Figure 8. Evolution of the local root mean square error of the three models, 1 (*blue*), 2 (*red*) and 3 (*green*) as a function of the Lin's distance Ψ_{Lin}. The colored shading represent the standard error of the mean associated to the local quadratic error of each model.

the three models. This indicates that each of the three models provide a similar description of the out of cusp magnetopause surface. It is not surprising to notice a slight increase of the local RMSE when for high values of Ψ_{Lin}, at the right of the black dashed line as the concerned events are likely to be located in the far nightside according to the average distribution of Ψ_{Lin} in the Figure 4. Coming closer to the near-cusp region and looking now at the region between the two dotted lines, we remark similar performances of the models 2 and 3 while the error is more important for the model 1. This shows that the indented models predict a more accurate position of the magnetopause than the non-indented one and thus,its actual indentation.

Finally, we notice a drastic enhancement of the local RMSE of the model 2 for the lowest values of Ψ_{Lin}.The only possible explanation consistent with the existence of the indentation stands in an underestimation of the position of the magnetopause by this model. This is confirmed by the Figure 9 that represents the evolution of the binned average error ΔR as a function of Ψ_{Lin}. For high Ψ_{Lin} values, and thus out of the near-cusp region, the similar evolution noticed for the three curves indicate the neutrality of each model regarding the prediction of the magnetopause radial distance for a given set of angular coordinates (θ, ϕ). For the lowest values of Ψ_{Lin}, the positive error confirms that the non-indented model one overestimates the position of the events of the test set. This confirms an actual indentation of the magnetopause. As the error of model three is close to 0 for every value of Ψ_{Lin}, we can infer that the indentation is consistent with the non-linear magnetohydrodynamic modeling previously made by Liu et al. (2015).

5. Characteristics of the Model

The results of the previous section provide arguments in favor of the existence of an indentation of the magnetopause consistent with the one observed in MHD simulations. Naturally, Model 3, described by Equations 2 and 4, constitutes a modification of the model developed by Nguyen et al. (2022c) accounting for this indentation. We then obtain a new magnetopause surface model parametrized by 5 different solar wind and seasonal parameters: the solar wind dynamic and magnetic pressures P_{dyn} and P_m, the IMF clock angle components, the Earth dipole tilt angle γ. A numerical implementation of this model, with the possibility to consider the indentation or not, can be found at https://doi.org/10.5281/zenodo.5668780.

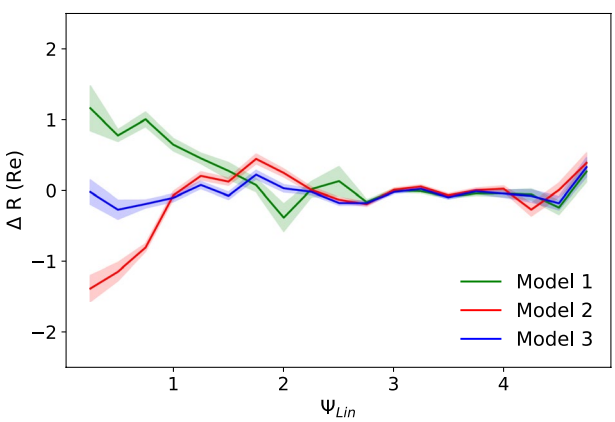

Figure 9. Evolution of the binned average error $\Delta R = R_{model} - R_{observed}$ of the three models, 1 (*blue*), 2 (*red*) and 3 (*green*) as a function of the Lin's distance Ψ_{Lin}. The colored shading represent the standard error of the mean associated to the local quadratic error of each model.

As it simply consists in the addition of an indentation term that vanishes outside of the near-cusp region, the stand-off distance and the flaring of this model are already described in Nguyen et al. (2022c). Consequently, we complete the details of our new model by presenting the characteristics of the indentation argument Q.

Figure 10 represents the value of Q computed in the northern hemisphere ($X - Z$) plane (e.g., $\phi = 0°$) for different solar wind and seasonal conditions. Looking at the first panel, an increasing dynamic pressure results in a narrower and shallower indentation. This is the consequence of an unchanged location of the polar cusps, as suggested by Zhou and Russell (1997) or Zhang et al. (2013), and an earthward motion of the magnetopause when the solar wind dynamic pressure increases. The second panel suggests a sunward motion of the indentation when the IMF turns from a northward to a southward position. This is consistent with the observational findings related to this dependency (Nguyen et al. [2022d] and references therein). Finally, the third panel suggests a seasonal motion of the indentation consistent with the one expected for the polar cusp. The same motion of the cusp that explains the increase of the northern hemisphere flaring during summer time (Nguyen et al., 2022c).

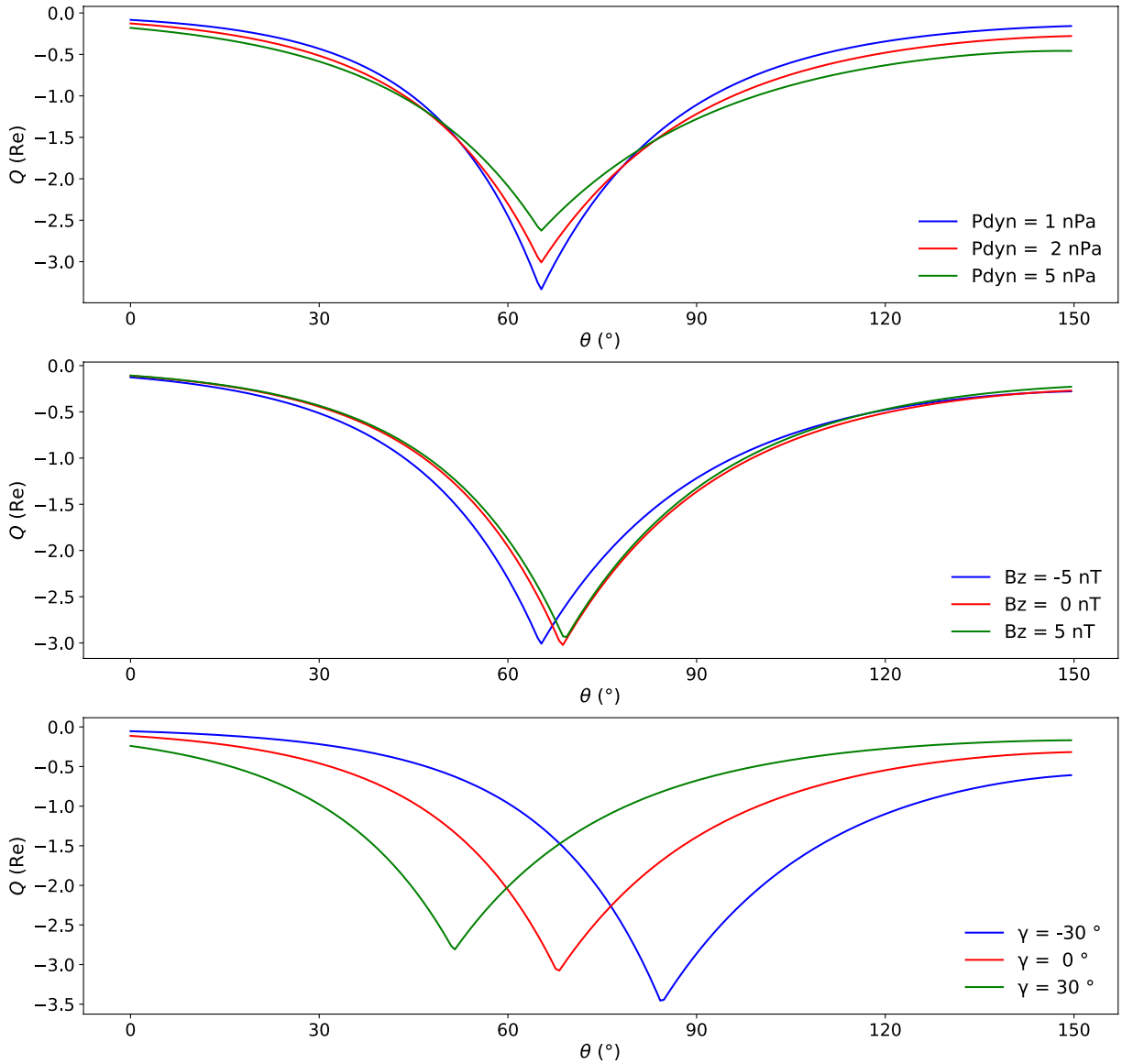

Figure 10. Evolution in the northern hemisphere (*X*–*Z*) plane of Q for three different solar wind and seasonal conditions: the dynamic pressure P_{dyn} (*upper panel*), the IMF B_z component (*middle panel*) and the Earth dipole tilt angle γ (*lower panel*). The default parameters used for the computation of Q are, when these features are not changing in the concerned panel, $P_{dyn} = 2$ nPa, $B_z = -2$ nT, $B_y = 0.01$ nT and $\gamma = 0°$.

6. Conclusion

The geometry of the polar cusps is described by two distinct boundaries. An inner boundary that separates the cusp region from the magnetosphere and an external boundary that corresponds to the magnetopause current-sheet outside of which resides the magnetosheath plasma.

The shape of the magnetopause at the cusp latitudes is still under debate as seen through numerous past studies, and the associated magnetopause surface models that account either for an indentation (Boardsen et al., 2000; Lin et al., 2010; Liu et al., 2015) or not (Jelínek et al., 2012; Lavraud, Fedorov, et al., 2004; Nguyen et al., 2022c; Shue et al., 1998).

In this paper, we compared the position of manually selected magnetopause cusp crossings with the position of out of cusp magnetopause crossings either obtained automatically or taken from a NASA database to address the question of the indentation.

At first, this comparison showed that one of the most detailed analytical description of this indentation (Lin et al., 2010) rather depicted the position of the cusp inner boundaries and not the magnetopause current sheet.

Second, this comparison, along with the fit of several magnetopause surface model suggests that the magnetopause is actually indented and that this indentation is consistent with that observed in MHD simulations (Liu et al., 2015).

These findings result in the production of a new asymmetric magnetopause surface model that accounts for this indentation.

From now on, the geometrical properties of the indentation could be further analyzed through the statistical analysis of the angular width and the radial distance of the near-cusp magnetopause for changing solar wind and seasonal conditions. Those additional findings may then be used to modify accordingly the expressions of the indentation term Q that we introduced to describe the indentation in our magnetopause surface model.

Data Availability Statement

THEMIS data are accessible via the NASA Coordinated Data Analysis web (https://cdaweb.sci.gsfc.nasa.gov/index.html/). Cluster and Double Star data are accessible via the Cluster and Double Star Science archive (http://csa.esac.esa.int/). All of our trained algorithms can be found here https://doi.org/10.5281/zenodo.5668298 (Nguyen, 2021a). The developed magnetopause models can be found here https://doi.org/10.5281/zenodo.5668780 (Nguyen, 2021b).

Acknowledgments
The authors thank the French Ministry of Defense for the funding of this work. The authors acknowledge the support of the THEMIS, Cluster, Double Star and MMS instrument and science team as well as Zdenek Němeček for the fruitful discussions and support.

References

Boardsen, S. A., Eastman, T. E., Sotirelis, T., & Green, J. L. (2000). An empirical model of the high-latitude magnetopause. *Journal of Geophysical Research: Space Physics*, *105*(A10), 23193–23219. https://doi.org/10.1029/1998ja000143

Frank, L. A. (1971). Plasma in the Earth's polar magnetosphere. *Journal of Geophysical Research*, *76*(22), 5202–5219. https://doi.org/10.1029/JA076i022p05202

Haerendel, G., Paschmann, G., Sckopke, N., Rosenbauer, H., & Hedgecock, P. C. (1978). The frontside boundary layer of the magnetosphere and the problem of reconnection. *Journal of Geophysical Research: Space Physics*, *83*(A7), 3195–3216. https://doi.org/10.1029/ja083ia07p03195

Heikkila, W. J., & Winningham, J. D. (1971). Penetration of magnetosheath plasma to low altitudes through the dayside magnetospheric cusps. *Journal of Geophysical Research*, *76*(4), 883–891. https://doi.org/10.1029/ja076i004p00883

Jelínek, K., Němeček, Z., & Šafránková, J. (2012). A new approach to magnetopause and bow shock modeling based on automated region identification. *Journal of Geophysical Research: Space Physics*, *117*(A5). https://doi.org/10.1029/2011ja017252

Lavraud, B., & Cargill, P. J. (2005). Cluster reveals the magnetospheric cusps. *Astronomy and Geophysics*, *46*(1), 1.32–1.35. https://doi.org/10.1046/j.1468-4004.2003.46132.x

Lavraud, B., Dunlop, M. W., Phan, T. D., Rème, H., Bosqued, J. M., Dandouras, I., & Balogh, A. (2002). Cluster observations of the exterior cusp and its surrounding boundaries under northward IMF. *Geophysical Research Letters*, *29*(20), 1995. https://doi.org/10.1029/2002GL015464

Lavraud, B., Fedorov, A., Budnik, E., Grigoriev, A., Cargill, P., Dunlop, M., & Balogh, A. (2004). Cluster survey of the high-altitude cusp properties: A three-year statistical study. *Annales Geophysicae*, *22*(8), 3009–3019. https://doi.org/10.5194/angeo-22-3009-2004

Lavraud, B., Phan, T., Dunlop, M., Taylor, M., Cargill, P., Bosqued, J., & Fazakerley, A. (2004). The exterior cusp and its boundary with the magnetosheath: Cluster multi-event analysis. *Annales Geophysicae*, *22*(8), 3039–3054. https://doi.org/10.5194/angeo-22-3039-2004

Lavraud, B., Rème, H., Dunlop, M. W., Bosqued, J.-M., Dandouras, I., Sauvaud, J.-A., & Keiling, A. (2005). Cluster observes the high-altitude CUSP region. *Surveys in Geophysics*, *26*(1–3), 135–175. https://doi.org/10.1007/s10712-005-1875-3

Lin, R. L., Zhang, X. X., Liu, S. Q., Wang, Y. L., & Gong, J. C. (2010). A three-dimensional asymmetric magnetopause model. *Journal of Geophysical Research: Space Physics*, *115*(A4). https://doi.org/10.1029/2009ja014235

Liu, Z., Lu, J. Y., Wang, C., Kabin, K., Zhao, J. S., Wang, M., & Zhao, M. X. (2015). A three-dimensional high Mach number asymmetric magnetopause model from global MHD simulation. *Journal of Geophysical Research: Space Physics*, *20*(7), 5645–5666. https://doi.org/10.1002/2014JA020961

Newville, M., Stensitzki, T., Allen, D. B., & Ingargiola, A. (2014). *LMFIT: Non-linear least-square minimization and curve-fitting for Python*. Zenodo. https://doi.org/10.5281/zenodo.11813

Nguyen. (2021a). *Gautiernguyen/in-situ_Events_lists: In-situ events list*, Zenodo. https://doi.org/10.5281/zenodo.5668298

Nguyen. (2021b). *Gautiernguyen/magnetopause_models: Magnetopause models*, Zenodo. https://doi.org/10.5281/zenodo.5668780

Nguyen, G., Aunai, N., Michotte de Welle, B., Jeandet, A., Lavraud, B., & Fontaine, D. (2022a). Massive multi-mission statistical study and analytical modeling of the earth magnetopause: 1. A gradient boosting based automatic detection of near-earth regions. *Journal of Geophysical Research: Space Physics*, *127*, e2021JA029773. https://doi.org/10.1029/2021JA029773

Nguyen, G., Aunai, N., Michotte de Welle, B., Jeandet, A., Lavraud, B., & Fontaine, D. (2022b). Massive multi-mission statistical study and analytical modeling of the Earth magnetopause: 2. Shape and location. *Journal of Geophysical Research: Space Physics*, *127*, e2021JA029774. https://doi.org/10.1029/2021JA029774

Nguyen, G., Aunai, N., Michotte de Welle, B., Jeandet, A., Lavraud, B., & Fontaine, D. (2022c). Massive multi-mission statistical study and analytical modeling of the Earth's magnetopause: 3. An asymmetric magnetopause analytical model. *Journal of Geophysical Research: Space Physics*, *127*, e2021JA030112. https://doi.org/10.1029/2021ja030112

Nguyen, G., Aunai, N., Michotte de Welle, B., Jeandet, A., Lavraud, B., & Fontaine, D. (2022d). Massive multi-mission statistical study and analytical modeling of the Earth's magnetopause: 4. On the near-cusp magnetopause indentation. *Journal of Geophysical Research: Space Physics*, *127*, e2021JA029776. https://doi.org/10.1029/2021ja029776

Šafránková, J., Němeček, Z., Dušík, v., Přech, L., Sibeck, D. G., & Borodkova, N. N. (2002). The magnetopause shape and location: A comparison of the interball and geotail observations with models. *Annales Geophysicae*, *20*(3), 301–309. https://doi.org/10.5194/angeo-20-301-2002

Shue, J.-H., Song, P., Russell, C. T., Steinberg, J. T., Chao, J. K., Zastenker, G., & Vaisberg, O. L. (1998). Magnetopause location under extreme solar wind conditions. *Journal of Geophysical Research: Space Physics*, *103*(A8), 17691–17700. https://doi.org/10.1029/98ja01103

Spreiter, J. R., & Briggs, B. R. (1962). Theoretical determination of the form of the boundary of the solar corpuscular stream produced by interaction with the magnetic dipole field of the earth. *Journal of Geophysical Research*, *67*(1), 37–51. https://doi.org/10.1029/jz067i001p00037

Zhang, B., Brambles, O., Lotko, W., Dunlap-Shohl, W., Smith, R., Wiltberger, M., & Lyon, J. (2013). Predicting the location of polar cusp in the lyon-fedder-mobarry global magnetosphere simulation. *Journal of Geophysical Research: Space Physics*, *118*(10), 6327–6337. https://doi.org/10.1002/jgra.50565

Zhou, X.-W., & Russell, C. T. (1997). The location of the high-latitude polar cusp and the shape of the surrounding magnetopause. *Journal of Geophysical Research: Space Physics*, *102*(A1), 105–110. https://doi.org/10.1029/96ja02702